

See discussions, stats, and author profiles for this publication at: <https://www.researchgate.net/publication/269987181>

Fabrication and Application of Catalytic Carbon Membranes for Hydrogen Production from Methanol Steam Reforming

ARTICLE *in* INDUSTRIAL & ENGINEERING CHEMISTRY RESEARCH · JANUARY 2015

Impact Factor: 2.59 · DOI: 10.1021/ie503094r

READS

31

6 AUTHORS, INCLUDING:



Bing Zhang

Shenyang University of Technology

19 PUBLICATIONS 151 CITATIONS

[SEE PROFILE](#)



Tonghua Wang

Dalian University of Technology

56 PUBLICATIONS 1,052 CITATIONS

[SEE PROFILE](#)



Jie Shan Qiu

Dalian University of Technology

440 PUBLICATIONS 7,303 CITATIONS

[SEE PROFILE](#)

Fabrication and Application of Catalytic Carbon Membranes for Hydrogen Production from Methanol Steam Reforming

Bing Zhang,*^{†,‡} Dandan Zhao,[†] Yonghong Wu,[†] Hongjing Liu,[†] Tonghua Wang,^{*‡} and Jieshan Qiu[‡]

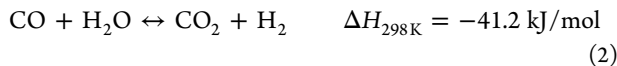
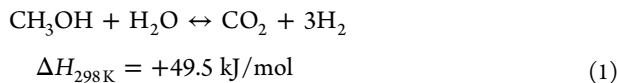
[†]School of Petrochemical Engineering, Shenyang University of Technology, 30 Guanghua Street, Liaoyang 111003, China

[‡]Carbon Research Laboratory, Liaoning Key Lab for Energy Materials and Chemical Engineering, State Key Lab of Fine Chemicals, School of Chemical Engineering, Dalian University of Technology, Dalian 116012, China

ABSTRACT: Novel catalytic carbon membranes (CCMs) were fabricated by a mixture of phenolic resin and nanosized copper-based catalyst as precursor, through the processes of blending, compressing, molding, and pyrolysis. The thermal stability of precursors was studied by thermogravimetric analysis. The surface morphology, carbon structure, pore structure, and catalytic reduction property of CCMs were characterized. The CCMs were applied to assembly reactors for the reaction of hydrogen production from methanol steam reforming. Comparative study of catalytic performance was made among the reactors of CCMs, traditional fixed bed, and inert carbon membranes. The methanol steam reforming in CCMs was investigated by some crucial operation variables, including reaction time, reactor configuration, streaming mode, space velocity, and molar ratio. Results have shown that the as-synthesized catalyst and CCMs are stable enough to tolerate the present reaction condition for a long life expectancy. Although the carbon matrix is favorable for dispersing and improving the effective exposure of copper-based catalyst to reactant, the distinct pore diffusion in CCMs is notable. The performance reaches 95% for methanol conversion and 92% for hydrogen yield when a CCM-assembled reactor is operated under the condition of two outlet streams, space velocity at 9.6 h⁻¹, and methanol/steam molar ratio of 1:1.

1. INTRODUCTION

Since hydrogen was identified as one of the highest potential clean energies in the 21st century, it has attracted much attention toward the development of various hydrogen production methods, including mineral fuel, electrolysis of water, microbionics, photocatalytic decomposition of water, etc.^{1,2} In comparison, the steam reforming of methanol (SRM) is more promising because of the advantages of easily available raw materials, simple process, mild reaction conditions, convenient operation, few byproducts, suitable setup scale, portability, and meeting the requirements of different end users.³ The global reaction of SRM can be written as eq 1. However, another two side reactions also exist, i.e., the water gas shift (eq 2) and decomposition of methanol (eq 3). The major challenge for SRM is to produce highly purified hydrogen with almost complete conversion of methanol for its applications (e.g., fuel cells) and cost effectiveness. Because all three reactions are reversible with the restriction of thermodynamic equilibrium constants of the chemical reactions, it is very difficult to substantially improve the methanol conversion and hydrogen selectivity in a traditional fixed bed using cheap copper-based catalyst.^{4–6}



In order to break through the restriction, membrane reactors have been utilized to shift the chemical equilibrium toward the right-hand side of the SRM reaction, relying on the successive removal of desired product H₂ from the system with the integrated selective membranes. In the membrane reactor, the most frequently used membrane material is palladium due to its extremely outstanding selectivity for H₂. However, some innate issues (such as high-cost, lower permeability, brittleness, etc.) have seriously prohibited the wide adaptability of palladium membranes. It is of great significance to develop alternative membranes, e.g., carbon membranes.^{7,8} It has been proved that carbon membrane reactors can produce higher methanol conversion or hydrogen recovery for the SRM reaction than the palladium membrane reactor and the traditional fixed bed.^{9–12} Nevertheless, there is still a possibility for the further improvement of the reaction efficiency by fairly modifying the integrated membrane materials.¹³ On the whole, all those carbon membrane reactors were assembled by inert carbon membranes that merely take the function of separation media during the reaction process. Studies have verified that porous carbon materials could significantly promote the mass transport of fluid in the reaction system, and consequently increase the reactivity and performance of catalyst when they are applied to the catalyst support.^{14,15}

In this regard, here we made an attempt to fabricate catalytic carbon membranes (CCMs) by incorporating nanosized catalyst into carbon membranes for the application of the

Received: August 2, 2014

Revised: December 20, 2014

Accepted: December 21, 2014

Published: December 21, 2014

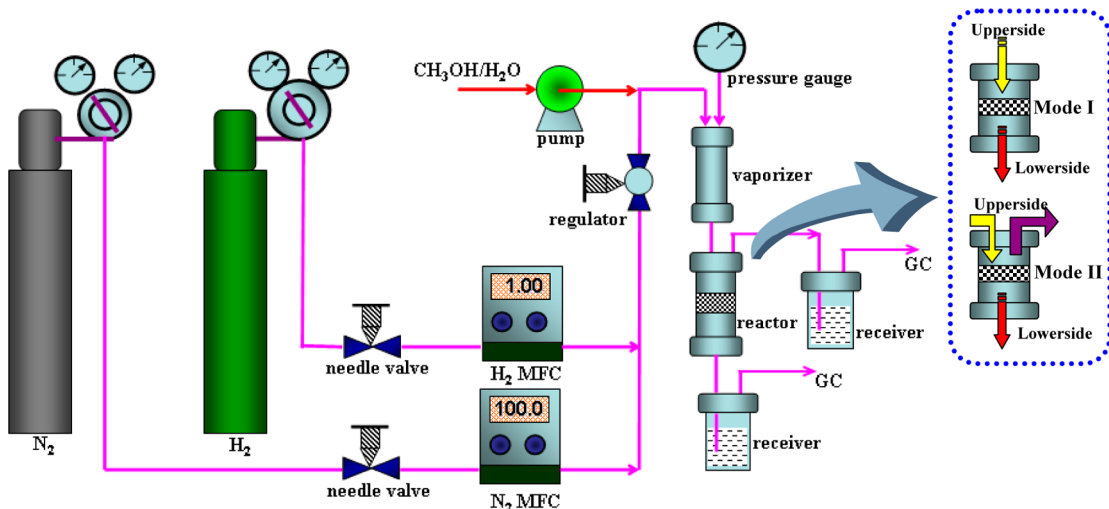


Figure 1. Schematic experimental setup for the reaction of methanol steam reforming.

SRM reaction. The motivations for the utilization of catalytic carbon membranes (CCMs) are to exert their two expectant functions on improving the conversion and selectivity: (1) allowing more reactive sites to participate the reaction by highly dispersing catalyst; (2) enhancing the mass and heat transfer of the reaction system through the abundant microreactor-like micropores.

2. EXPERIMENTAL SECTION

2.1. Materials. The main raw material is commercial phenolic resin procured from Liaoyang Qianjin Chemical Engineering Factory, China. The other materials include the curing agent hexamethylenetetramine (HMTA, analytic grade) and additive methyl cellulose (industrial grade).

Before fabrication, the phenolic resin was subjected to partial curing in order to create a large amount of porosity in the resultant carbon membranes. The curing was performed by heating the powder mixture of 30 g of faint yellow phenolic resin and 2.4 g of HMTA at 150 °C for 1 h. After that, the cured phenolic resin with a dark brown foaming appearance was ground into fine powder, with an average particle diameter of around 0.3 μm.

2.2. Fabrication of Catalytic Carbon Membranes (CCMs). First of all, nanosized Cu/ZnO/Al₂O₃ catalyst was prepared by the coprecipitation method. Three aqueous solutions were made by respectively dissolving analytical grade starting materials copper nitrate, zinc nitrate, and aluminum nitrate into distilled water, in a molar ratio of Cu:ZnO:Al₂O₃ equaling 70:15:15. At the same time, Na₂CO₃ solution was also made according to the stoichiometric coefficient of reactions with the above three metal nitrates. Next, the three nitrates were mixed under vigorous stirring for 30 min at 60 °C. The formed mixture was dropwise added to Na₂CO₃ solution with stirring over 30 min to completely finish the reaction, followed by settling for another 6 h. Then, a filter cake with the color of pale green was yielded through the deposition and filtration of the as-formed liquor. After washing with distilled water at 50 °C to remove remaining Na⁺, the neutral cake was further dried at 110 °C for 24 h to eliminate residual water, and calcined at 320 °C for 3 h. Finally, a fine powder of dark brown Cu/ZnO/Al₂O₃ catalyst was obtained.

The fabrication of CCMs was conducted by three steps: dough formation, molding, and pyrolysis. First, a uniform pasty

dough was formed by successively kneading a mixture for about 1 h, which was comprised of the as-prepared catalyst powder, the cured phenolic resin powder, methyl cellulose, and suitable deionized water. After aging at ambient temperature for 80 min in a closed container, the dough was divided into small fractions of about 2.5 g and pressed into a disk-shaped membrane with a diameter of ca. 3 cm and a thickness of ca. 5 mm. Then, the nascent membranes were naturally dried in a dark room for 5–7 days to avoid any crack formation. The following pyrolysis was carried out from ambient temperature to 400 °C at a heating rate of 2 °C/min and holding at 400 °C for 3 h, then ramped to 600 °C at 1 °C/min and holding at 600 °C for 1 h, before cooling to room temperature. The inert pyrolysis atmosphere was kept by purging the furnace with highly purified nitrogen at 100 mL/min from beginning to end. Ultimately, CCMs were obtained with a diameter of around 2.5 cm and a thickness of 3.5 mm. It was estimated that each CCM contains about 0.3 g of copper-based catalyst over the whole weight of ca. 1.0 g.

For comparison, inert carbon membranes (ICMs) were also prepared analogously to the procedure and conditions of CCMs, without the incorporation of catalyst.

2.3. Characterization. A USA PE TGA-4000 thermogravimetric analyzer was adopted to evaluate the thermal stability of precursors by recording the function of weight remaining with the pyrolysis temperature. The testing conditions were set as a nitrogen flow rate of 20 mL/min and a temperature range of 30–800 °C at a heating rate of 20 °C/min.

Temperature-programmed reduction (TPR) is a common tool for the characterization of metal oxides dispersed on a support. Here, a Micromeritic AUTOCHEM II 2920 chemisorption analyzer was adopted to record the H₂-TPR profiles of CCMs in order to gain insight into the quantitative information on the reducibility of the oxide's surface with hydrogen, as well as the heterogeneity of the reducible surface.

The microstructural morphology of CCMs was observed by scanning electron microscopy (SEM) and transmission electron microscopy (TEM). They were correspondingly conducted by a JEM 7500F cold field-emission SEM with energy dispersive spectrometry (EDS) microanalysis and a JEM-2100 TEM from JEOL.

The carbon structure was identified by a Rigaku D/max2500 for X-ray diffraction (XRD) with Cu K α radiation ($\lambda = 1.54\text{ }178\text{ \AA}$) under the operating conditions of 40 kV and 80 mA.

The pore size distributions for macropores and meso- and micropores of CCMs were measured by a bubble point method^{16,17} and nitrogen adsorption technique, respectively. Prior to the measurement of nitrogen adsorption, all the samples were degassed at 300 °C for at least 3 h. Adsorption–desorption isotherms were procured with varying the ratio of adsorption pressure over ambient pressure at liquid nitrogen temperature (−196 °C) by a Micromeritics ASAP 2420 instrument. Based on the isotherms and standard calculation methods, BET specific surface area, pore volume, and pore size distribution were obtained.

The apparent porosity referring to the percentage of the open pore volume (the pores connecting with atmosphere) over the total pore volume was detected by a boiling method in the China National Standard GB/T 1966–1996.¹⁸

2.4. Methanol Steam Reforming Reaction. Figure 1 shows the schematic experimental setup for SRM reaction. Three reactor configurations assembled by catalyst fixed bed (FB), ICMs, and CCMs, were respectively denoted as R-FB, R-ICM, and R-CCM. The R-FB was packed with 1.0 g of catalyst mixing with an equal weight of quartz sand (40 mesh in size) in the central part of a stainless tube (2.1 cm i.d., 30 cm length), while the R-ICM and R-CCM were divided into two parts (i.e., upper side and lower side) by the embedded carbon membranes.

The temperature of the vaporizer was kept at 110 °C throughout the reaction, while that of the reactor was automatically controlled by a programmable temperature controller from beginning to end. The program of the reactors was set as first heating from ambient temperature to 180 °C at a rate of 1 °C/min with the sweeping of 100 mL/min flowing nitrogen, and then dwelling at 180 °C for 5 h to in situ activate the catalyst under the purging of 110 mL/min H₂/N₂ mixed gas (1:10 vol/vol). After activation, the temperature of the reactor was further elevated to 240 °C at 1 °C/min under 100 mL/min flowing nitrogen atmosphere. Reactant methanol/water mixture was continuously fed into the vaporizer by an HPLC LC-01P microsyringe pump (Johnson Inc. of China) under atmospheric pressure. In this work, the weight hourly space velocity (WHSV) was varied in the range 7.2–12.0 h^{−1} by tuning the feed flow rate of the reactant. The product released from the outlet of the reactor was condensed and collected by a stainless steel reservoir, in which the residual methanol and water were absorbed into distilled water while the gas species were directed to a gas chromatograph (GC) by a six-path valve. The GC (7890II, TECHCOMP (HOLDINGS) Ltd.) was equipped with a TDX01 packed column. The amount of unconverted methanol in collected liquid was analyzed using a hydrogen flame ionization detector (GC9790II, Zhejiang FULI Analytical Instrument Co., Ltd., China) with a KB-5 capillary column (30 m × 0.25 mm × 0.5 μm). According to the following equations (eqs 4 and 5), the methanol conversion ($X_{\text{CH}_3\text{OH}}$) and hydrogen yield (Y_{H_2}) could be calculated.^{10,12,19}

$$X_{\text{CH}_3\text{OH}} = \frac{n_{\text{CH}_3\text{OH}_{\text{in}}} - n_{\text{CH}_3\text{OH}_{\text{out}}}}{n_{\text{CH}_3\text{OH}_{\text{in}}}} \cdot 100\% \quad (4)$$

$$Y_{\text{H}_2} = \frac{n_{\text{H}_2,\text{out}}}{3n_{\text{CH}_3\text{OH}_{\text{in}}}} \cdot 100\% \quad (5)$$

where the subscripts “in” and “out” represent the molar flow rates of the specified reactant inlet and product outlet of the reactor, respectively.

3. RESULTS AND DISCUSSION

3.1. Thermal Stability of Precursors. The thermal weight remaining profiles as a function of pyrolysis temperature are shown in Figure 2. Note that the precursor of ICMs exhibits

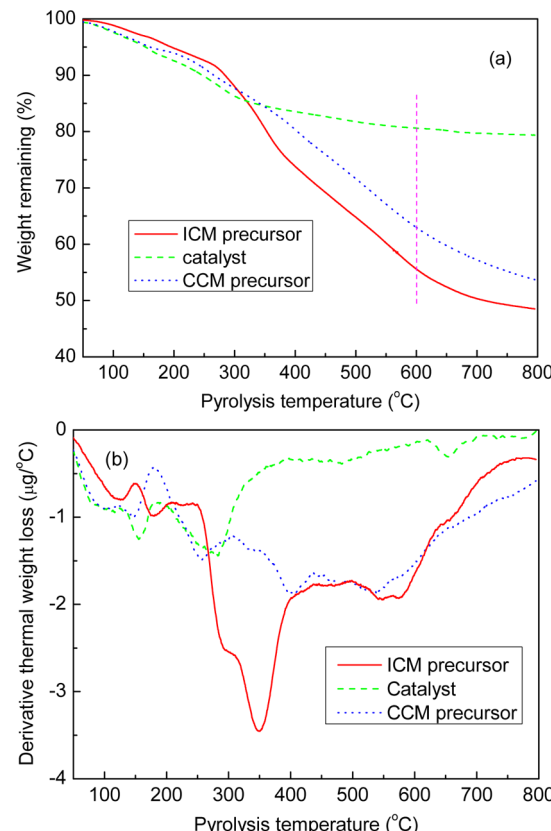


Figure 2. Thermal stability analysis of precursors. (a) Weight remaining curves and (b) their derivative curves.

four obvious thermal weight loss stages: ~150, 150–250, 250–450, and 450–700 °C. In the first stage, the weight loss is mainly contributed by the release of remaining water and vapors derived from the further curing reactions of partially cured phenolic resin.²⁰ The second weight loss stage might be due to the thermal decomposition of methyl cellulose in the precursor.²¹ The third stage is owing to the release of small pyrolytic fragments formed by the cleavage of methylene bridged phenolic ring structure and the intermediates of the complicated curing reaction. It results in the generation of hydroxymethyl and methylene ether groups, oxymethylene species, and a small amount of oxidation products of formaldehyde liberated from the decomposition of the ether intermediates of the curing reaction.²² With the temperature increasing to the fourth stage, some large fragments would be evolved and would escape from the matrix as the result of the thermal decomposition of the main molecular backbone.²³

The present Cu/ZnO/Al₂O₃ catalyst has three thermal weight loss stages: 100–200, 200–350, and 600–750 °C, corresponding to (1) the evaporation of absorbed water or gases trapped in catalyst, (2) the release of CO₂ originated from the decomposition of carbonates into oxides, and (3) the

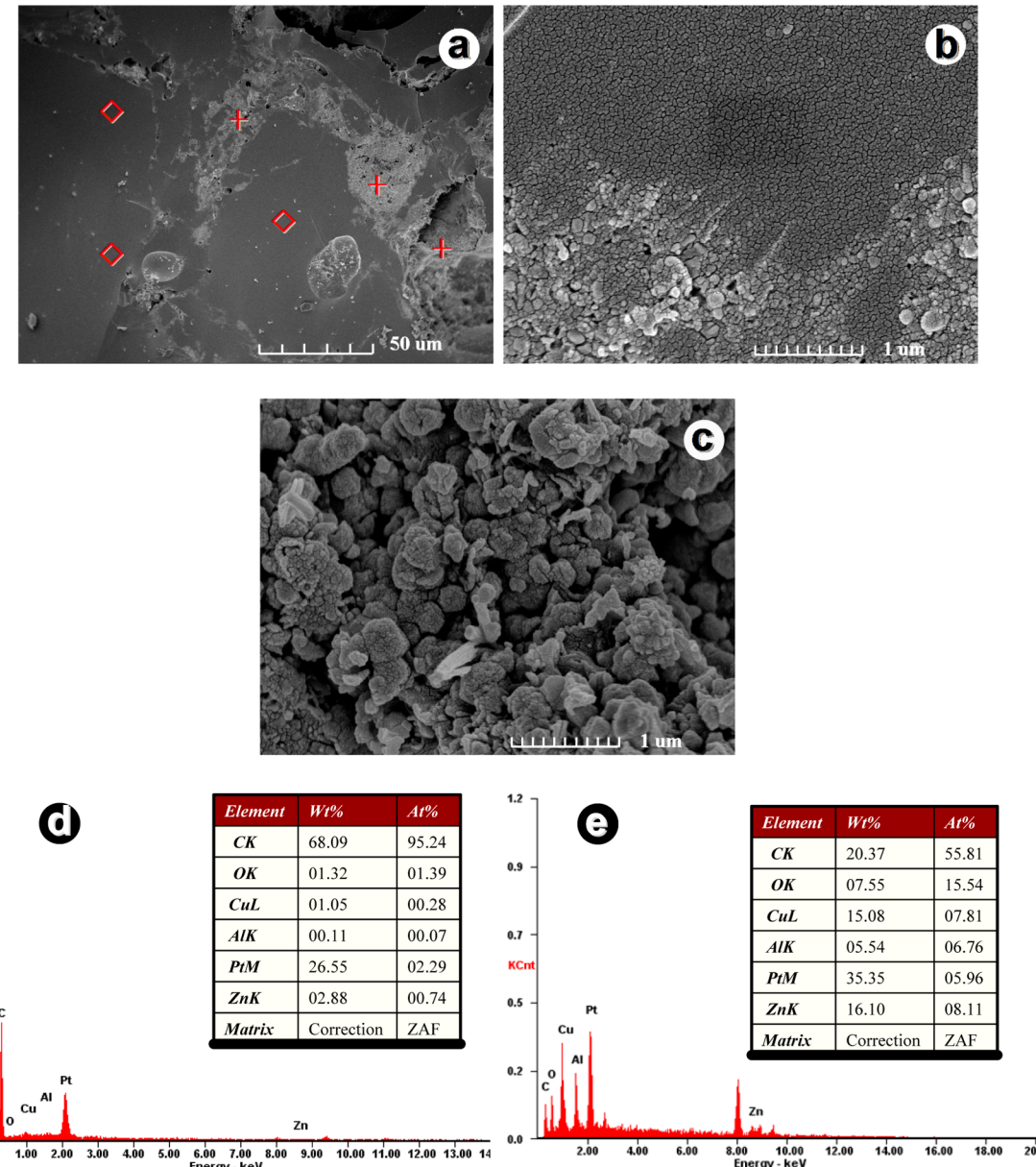


Figure 3. FE-SEM images of the catalytic carbon membranes. (a) Global surface view, magnification of (b) the location marked by diamonds and (c) the location marked by plus signs, and EDS spectra of (d) the location marked by diamonds and (e) the location marked by plus signs.

removal of some gases derived from the transition of crystal structure in oxides.

Because the precursor of CCMs is composed by the precursors of ICMs and Cu/ZnO/Al₂O₃ catalyst, the weight loss profile for the precursor of CCMs shows their conjunction results. That is, the thermal weight loss curve almost locates in the overlapping area of the latter two profiles throughout the temperature range as shown in Figure 2a. At the pyrolysis temperature of 600 °C, the weight remaining values are 55.5% for ICM precursor and 63.0% for CCM precursor, showing that the addition of catalyst increases the general thermal stability of the precursor. Nevertheless, it must be pointed out that the peak positions of 124.3 and 179.1 °C for ICM precursor respectively shift to 98.9 and 146.5 °C for CCM precursor, as shown in Figure 2b. The reason might be that the inclusion of metal oxides, CuO, ZnO, and Al₂O₃, perturbs the van der Waals interaction between the precursor molecular chains.²⁴ Consequently, the curing of phenolic resin and decomposition of

methyl cellulose reactions for CCM precursor may be modified to some extent at the early stage of pyrolysis.

Overall, the addition of catalyst to precursor does not obviously affect the individual properties and structures of catalyst and carbon matrix. Therefore, it is speculated that the activity of catalyst should be retained well in the membrane matrix, which is significant for the accomplishment of subsequent SRM reaction.

3.2. Morphology Observation. Figure 3 shows the field emission scanning electron microscopy (FE-SEM) images and EDS spectra of CCMs. From Figure 3a,b, we can see that the membrane surface is generally smooth with locally bright domains on occasion. The bright domains are formed by the stacking of particles with a diameter of several hundreds of nanometers (Figure 3c). As shown in the EDS result (Figure 3d), the predominant element is carbon with a content of 95.24 mol % in the dark domains, along with other minor elements, i.e., Cu, Al, Zn, and O. In contrast, the carbon content of 55.81

mol % is much lower in the bright domains, leading to the substantial increase of the other contents of O, Cu, and Zn, as shown in Figure 3e. According to the element contents, it is deduced that the particles in bright domains are identified as the copper-based catalyst.

TEM observation was also employed to gain insight into the existing state of the catalyst in the carbon matrix at the microscale level. Figure 4a shows the macroscopic view of

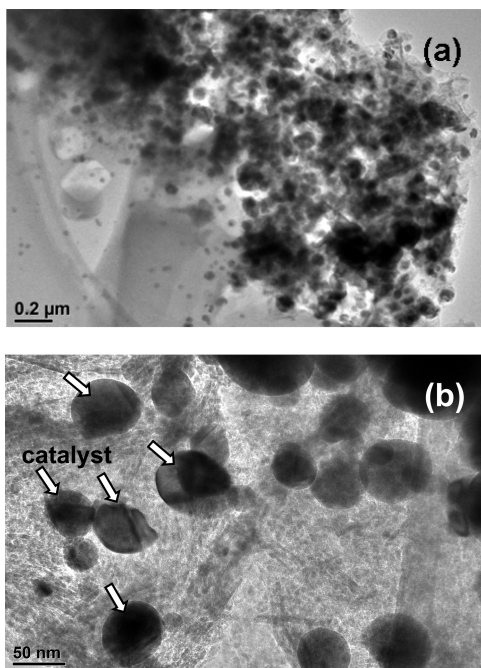


Figure 4. TEM images of catalytic carbon membranes embedded with uniform catalyst particles.

CCMs. The dispersed dark dots are catalyst particles. In a close-up view (Figure 4b), semicircular catalyst particles with a diameter of around 50 nm could be obviously found in the carbon matrix. Such a dimension for the catalyst is favorable for the dispersion in the membrane matrix and the enhancement of reaction activity.²⁵ Thereby, the TEM justifies that most of the catalyst is in the state of dispersion except for a few local aggregations on the membrane surface as shown in previous SEM images. The legible metal lattice in TEM also illustrates that the crystallite of catalyst remains intact. The clear boundary of catalyst particles suggests there is no serious encapsulation coke formation covering the CuO/ZnO/Al₂O₃ particle surface in the fresh CCMs, which is the major cause for the deactivation of copper-based catalyst.^{26,27} The reason is that the existence of Cu species in catalyst can suppress the coke formation by creating activated oxygen and forming coke gasification during the reaction, leading to a long-time stable activity.^{28,29} Actually, it cannot absolutely prevent the carbonaceous deposition in CCMs due to the evolution of various intermediates, including the coke precursors, during the pyrolysis of CCM precursor.^{30,31} Therefore, it does not exclude the formation of other types of coke in CCMs. On the whole, it shows that the carbon matrix has no seriously adverse effect on the catalyst. In return, the porous carbon matrix surrounding the catalyst affords an increase of the diffusivity of reactant through the membrane matrix and the preferential contacting

of reactant with the active sites of catalyst. In this way, CCMs are anticipated to intensify the reaction process.

3.3. Porous Structure Analysis. Figure 5 gives the nitrogen adsorption–desorption isotherms and their derived

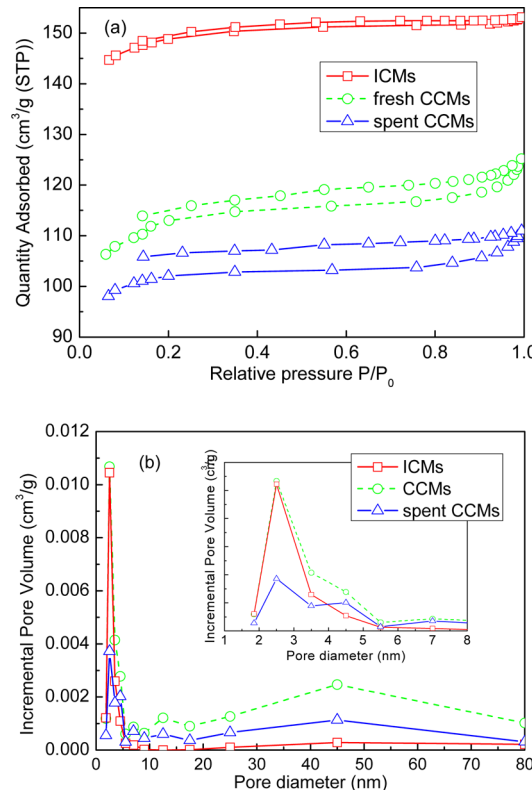


Figure 5. Pore characterization of carbon membranes from nitrogen adsorption–desorption technique. (a) Adsorption–desorption isotherms; (b) pore size distributions.

pore size distributions (PSDs). The hysteresis loops in the isotherms of the ICMs and CCMs imply their coincident type IV pore classification promulgated by IUPAC. In the range of relative pressure 0–0.2, the adsorption amount increases rapidly with the pressure. Then, the increasing tendency slows down gradually with the relative pressure ongoing from 0.2 to 0.9. When the relative pressure is up to 0.9–1.0, the increasing trend promptly elevates again. In order to gain insight into the structural changes of CCMs after reaction (reaction temperature 240 °C, MeOH/H₂O of 0.56:1, and S_V of 7.53 h⁻¹), the results of ICMs and spent CCMs are also shown in Figure 5 and Table 1.

Table 1. Porous Structure Information of Carbon Membrane Samples

item	Cu/ZnO/ Al ₂ O ₃	ICMs	fresh CCMs	spent CCMs
BET sp. surf. area, m ² /g	72	498	382	343
t-plot micropore vol., m ³ /g	0.001	0.204	0.134	0.136
mean pore diam, nm	—	1.90	1.99	1.98
porosity, ^a %	—	39.64	31.37	27.79

^aThe value refers to apparent porosity measured by the China National Standard GB/T 1966–1996.³¹

Figure 5a shows that ICMs possess substantially higher adsorption amounts than CCMs at the same relative pressure. As listed in Table 1, ICMs are 30.4% larger in BET specific surface area and 52.2% higher in microporous volume than CCMs, justifying the drop of porosity after the addition of nearly nonporous catalyst. After reaction, the micropore volume of CCMs is nearly intact, together with the specific surface area slightly decreasing. This implies that the main structure of CCMs is stable enough to tolerate the reaction conditions except for minor carbon deposition or mass filling in CCMs.

As shown in Figure 5b, the three similar PSD profiles concentrate around 1.9 nm, suggesting that the micro- and mesoporous structure is not obviously influenced by the incorporation of catalyst or reaction. At the same time, also notice that CCMs and spent CCMs have an additional PSD peak around 45 nm, revealing that the addition of catalyst contributes more macropores to the carbon membrane matrix due to the existence of a large amount of holes formed by the stacking of catalyst particles.

The apparent porosities shown in Table 1 could also verify the aforementioned reduction effect on the BET specific surface area and pore volume from nitrogen adsorption, by introducing nonporous solid catalysts into carbon membranes. The porosity of CCMs is further diminished from 31.37 to 27.79% after reaction. A possible reason is the occurrence of carbon deposition or mass filling in the porous channels of CCMs, resulting in the blockage of the porous structure of spent CCMs.^{23,32}

3.4. Microstructural Analysis. In the XRD patterns (Figure 6), the typically broad reflectance peak around 18–

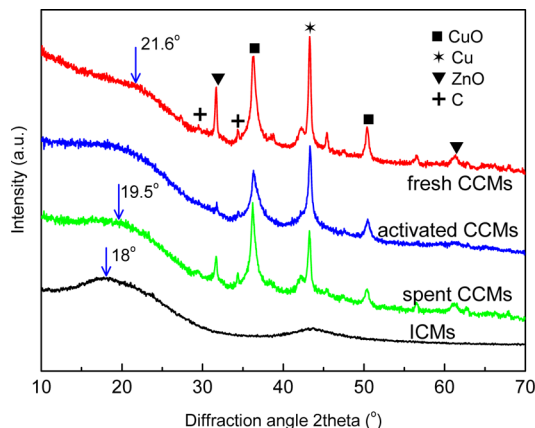


Figure 6. XRD patterns of catalytic carbon membranes.

23° is ascribed to the diffraction of the (002) plane for carbon materials. Some characteristic diffraction peaks could be identified representing CuO at 36.1 and 50°, Cu at 42°, and ZnO at 31.7 and 61.7° in fresh CCMs.^{25,33,34} The weak peaks at 29.5 and 34.4° are the clue for carbonaceous deposition,²⁸ which might be originated from the intermediates derived from the thermal degradation of carbonaceous precursors of CCMs during pyrolysis as analyzed in section 3.2. After the exclusion of encapsulation coke, it is deduced that the present carbonaceous deposition is probably ascribed to graphite layers distributed in the matrix of CCMs.³⁵ This type of coke formation should not give rise to any adverse effect on the catalytic activity of CCMs but diffusion resistance of fluid in the reaction system.

For activated CCMs that were pretreated at 180 °C by hydrogen for 5 h, the peaks representing deposited carbon are completely missing, together with the intensity reduction of ZnO. This may be the result of the reduction for ZnO to evolve into activated species Zn after hydrogen pretreatment for 5 h.^{28,36}

In comparison to fresh CCMs, the peak position of (002) diffraction for spent CCMs has shifted toward the direction of lower degree by 2°. Moreover, the (002) diffraction profile of spent CCMs becomes more narrow and symmetric. This implies that the microstructure of CCMs has been changed after reaction. This could be evidenced by the interlayer distance d_{002} values and diffraction peak intensity, namely, the increase of the d_{002} value from 0.411 to 0.455 nm, and the attenuation of diffraction peak intensity to a certain degree. In addition, it shows that the peaks for carbonaceous deposition are more obvious for spent CCMs, which agrees well with the analysis in nitrogen adsorption.

3.5. H₂-TPR Measurement. In the H₂-TPR spectra (Figure 7), the peak position indicates the temperature corresponding

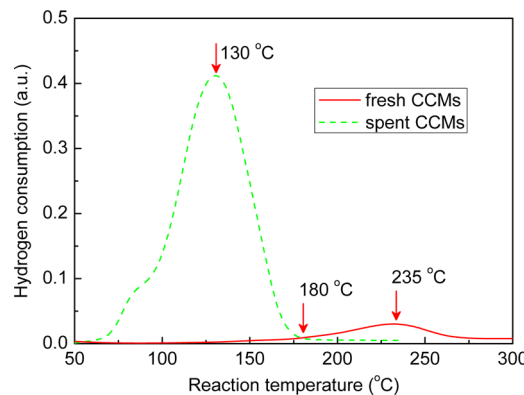


Figure 7. H₂-TPR of catalytic carbon membranes before and after reaction.

to the maximum rate of reduction. For fresh CCMs, the hydrogen consumption widely ranges from 125 to 275 °C. This indicates the coexistence of several states of CuO in the system, including highly dispersed CuO microcrystal, embedded Cu²⁺ in the crystal lattice of ZnO/Al₂O₃, and block CuO in the bulk phase.^{37–40} The peak position of CCMs locating at 235 °C is comparable to the value of 180–280 °C in the report for copper-based catalyst,⁴¹ which means the highest reducibility at this temperature. This temperature would be beneficial for complete methanol conversion of the SRM reaction by the catalyst of Cu/ZnO/Al₂O₃ and for the suppression of the undesired reverse water gas shift reaction and decomposition of methanol.^{42,43} Therefore, the selection of reaction temperature at 240 °C is appropriate for the present CCMs. In addition, it also implies that the incorporation does not significantly affect the catalytic performance of embedded copper-based catalyst in terms of the active sites serving as attacking points of hydrogen. On the contrary, the porous carbon matrix might be favorable for the reaction by providing good dispersion of catalyst. For spent CCMs, the maximum amount of hydrogen consumption increases about 10 times, along with the peak position shifting toward a lower temperature to 130 °C. This indicates that the interaction between copper and support in CCMs decreases after reaction.⁴⁴ The change in the interaction between copper and the support can also be confirmed by the variation of XRD

peak intensities (Figure 6), namely the increase of CuO and the decrease of Cu after reaction. In addition, the remarkable improvement of the reducibility for spent CCMs may be associated with the promotion of activated O₂ molecules originated from the Cu species during the chemical reaction,^{45,46} and the contribution of ZnO (including a quasi-two-dimensional layer epitaxially developed over the ZnO support and small copper metal clusters dispersed over the ZnO).⁴⁷

3.6. Activity and Stability of Catalyst. The activity and stability of the as-prepared catalyst were studied in the R-FB at atmospheric pressure and 240 °C with S_V of 7.53 h⁻¹. Seen from Figure 8, after a short introduction period for 60 min, the

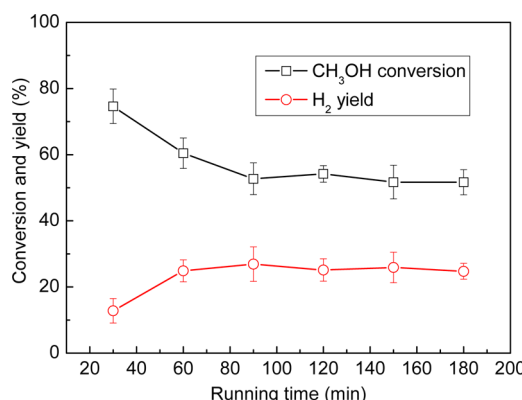


Figure 8. Effect of reaction time on methanol steam reforming in a fixed bed reactor (reaction temperature 240 °C, MeOH/H₂O of 0.56:1, and S_V of 7.53 h⁻¹).

present catalyst stably catalyzes hydrogen formation over 180 min, with a steady-state methanol conversion of 52% and a hydrogen yield of 25%. The data fluctuation during the early introduction period is due to the inhomogeneous distribution of reactant fluid passing through the entire reactor, resulting in the retarding effect of the product outlet of the reactor. The present methanol conversion is comparable to the data in the literature as listed in Table 2,^{5,9,12,13,48–51} illustrating the practicability of the as-synthesized catalyst. Besides, it also finds that the catalyst activity keeps well until to the end time of 180 min by retaining stable conversion and yield values. This indicates that the as-prepared catalyst is good in activity and stability for a long life expectancy.

3.7. Effect of Reactor Configuration. Table 2 also lists the results of the the SRM reaction in R-ICM and R-CCM

under the reaction temperature of 240 °C for 180 min. Compared to R-FB, R-ICM and R-CCM exhibit about 1.88-fold larger methanol conversion in magnitude. Simultaneously, the hydrogen yields increase by 3.8 times for R-ICM and 3.6 times for R-CCM. The intensification of SRM for R-ICM agrees well with reports in the literature.^{9,12} Table 2 shows that R-CCM exhibits a higher conversion of 97.78% and a lower hydrogen yield of 90.64% than R-ICM, suggesting that they intensify the SRM reaction in dependence on different mechanisms. For R-ICM, the enhancement is achieved by shifting the thermodynamic equilibrium toward the right-hand direction of SRM with the selective removal of the desired product H₂ via the integrated carbon membranes. Different from the extractor-like function of R-ICM, R-CCM takes the function of distributor and contactor associated with the intensification of uniform dispersion of catalyst and the heat and mass transfer of reactant.⁵² In future work of CCMs, the exposed catalyst on the membrane surface should be finely controlled for the adverse effect to shape the selectivity of catalyst.⁵³

The effect of streaming mode was also studied on the SRM reaction by varying the reactor configurations of R-CCM. Here, two types of streaming mode were adopted as shown in Figure 1. For mode I, one reactant stream was fed into R-CCM with one product stream outlet from the reactor at the lower side. The product was collected by a reservoir containing distilled water to absorb unconverted methanol and steam so as to give off incondensable gases H₂, CO, and CO₂. For mode II, an additional outlet stream was attached on the upper side at a gas flow rate of 5 mL/min in order to diminish the negative effect of retention. Similarly, the outlet stream of the upper side was also collected by a water-containing reservoir. From the comparative result given in Table 2, it was found that mode II shows a 2.1% higher methanol conversion with a somewhat reduction of H₂ yield than mode I. The reason probably lies in the different intensification ways of reaction. In mode II, a small portion of methanol and hydrogen would be inevitably entrained by the stream of carrier gas flowing out of the reactor at the upper side, apart from the expectant discharging from the lower side of the reactor. The adoption of mode II is equivalent to reducing the effective space velocity, giving rise to more possibility for the reactant contacting with catalytic active sites. This certainly improves the resultant methanol conversion. Actually, a fair comparison between mode I and mode II should be done at close conversion regardless of their space velocities. It shows that mode II exhibits a higher H₂ yield of 93.2% than mode I (90.64%) when the conversion of mode II

Table 2. Comparison of the Methanol Conversion and Hydrogen Yield of SRM

	reactor configuration (streaming mode)												
	R-FB	R-FB	R-FB	R-FB	R-FB	R-FB	R-ICM	R-FB	R-ICM	R-FB	R-CCM (mode I)	R-CCM (mode II)	R-CCM (mode II)
methanol convy, %	46.4	60	92	48.6	65	78	93.3	49	55	52	97.77	97.78	99.84
H ₂ yield, %	—	—	—	—	—	—	74.0	71	75	25	94.77	90.64	83.09
reaction temp, °C	250	260	250	240	230	240	225	250	250	240	240	240	240
source ^b	48	49	50	51	13	5	9	12	12	this work ^c	this work ^c	this work ^c	this work ^a

^aReaction conditions: catalytic carbon membranes, at 240 °C, 9.6 h⁻¹ (WHSV), and MeOH/H₂O of 0.56:1. ^bThe listed data in the references were adapted from the condition of Cu/ZnO/Al₂O₃ catalyst (coprecipitation method or commercial supply) and the reaction temperature of 225–260 °C. ^cReaction conditions of this work: catalytic carbon membranes, at 240 °C, 7.2 h⁻¹ (WHSV), and MeOH/H₂O of 0.56:1.

Table 3. Kinetic Analysis of SRM in Different Reactors^a

	reactor configuration (streaming mode)				
	R-FB	R-ICM	R-CCM (mode I)	R-CCM (mode II)	
$r_{SRM} \times 10^{-5}$, mol/(s·g)	$\alpha = 0.27$ $\alpha = 0.65$	1.46 1.26	1.44 0.55	1.44 (4.8 ^b) 0.55 (1.8 ^b)	0.75 (2.5 ^b) 0.12 (0.4 ^b)

^aReaction conditions: catalytic carbon membranes, at 240 °C, 7.2 h⁻¹ (WHSV), and MeOH/H₂O of 0.56:1. ^bThe values in parentheses are obtained by normalizing the effective amount of Cu/ZnO/Al₂O₃ in CCMs.

(96.6%) is close to that of mode I (97.78%). Therefore, mode II was adopted as the optimal streaming mode in sections 3.8 and 3.9.

Furthermore, an expression of the reaction rate (eq 6) was also utilized to investigate the kinetics of SRM reaction in CCMs.³⁴

$$r_{SRM} = kP_{CH_3OH}^\alpha$$

$$= \frac{F_{CH_3OH}^0 (1 - X_{CH_3OH})^\alpha - (a - X_{CH_3OH})}{w_m} \quad (6)$$

In eq 6, r_{SRM} is the reaction rate, mol/(s·g), $F_{CH_3OH}^0$ is the inlet methanol flow (mol/s), w_m is the mass of catalyst (g), α is the reaction order (0.65 for Cu, 0.27 for CuO), and X_{CH_3OH} is the methanol conversion. As listed in Table 3, the reaction rates of the present work fall in the range of literature reports.³⁴ The discrepancy among the reaction rates of different configurations can be correlated with the specific surface area of catalyst as proposed by Valdés-Solís et al., that is, larger specific area of catalyst gives rising to higher reaction rates.³⁴ Considering the composition of copper-based catalyst in CCMs is about 33%, it is reasonable to see that the CCMs possess somewhat inferior reaction rates. The underlying reason might be the reduction of the pore diffusion rate for reactant in CCMs by the resistance of the membrane matrix. This leads to the increase of the Thiele modulus (φ)

$$\varphi = L \left(\frac{k_p}{d_e} \right)^{1/2} = \left(\frac{\text{surface reaction rate}}{\text{pore diffusion rate}} \right)^{1/2}$$

and consequently subjects the global reaction to the pore diffusion to some extent. Therefore, it is concluded that the pore diffusion could not be ignored although the CCMs are favorable for the dispersion of catalyst in the membrane matrix and the exposure of active sites to the reactant. The resistance of pore diffusion in CCMs should be diminished by reducing the membrane thickness or increasing the porosity (or pore diameter) of CCMs. One can notice that the reaction rates for R-CCM are much higher than those for the other reactors when they are normalized by the effective amount of copper-based catalyst in CCMs, as shown in Table 3. This proves that the CCMs could significantly intensify the SRM reaction.

Moreover, the methanol conversions from several newly developed reactors were also selected from the literature to evaluate the R-CCM, namely, 78% for the isotherm fixed-bed reactor,⁵ 91.95% for the fluidized bed reactor,⁵⁴ and 96.26% for the coating bed of uniform distribution.⁵⁵ It is found that the present R-CCM can compete well with them. Therefore, it shows that the present R-CCM provides a new kind of promising reactor for SRM.

3.8. Effect of Space Velocity. The space velocity (S_V) is tightly connected to the residence time of reactant in the reactor. As shown in Figure 9, the methanol conversion reduces

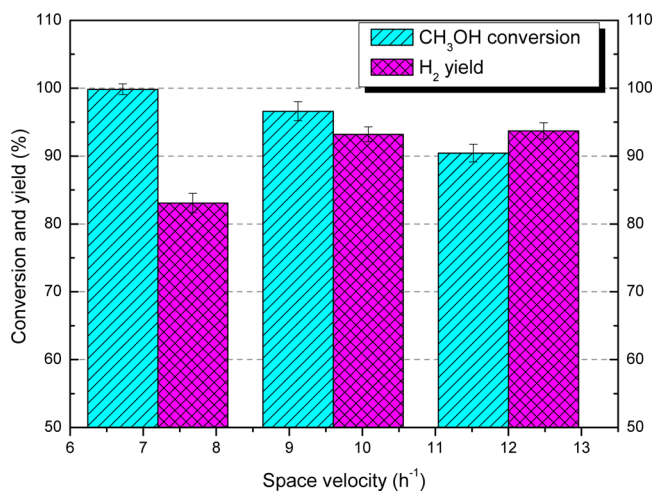


Figure 9. Effect of weight hourly space velocity on the reaction (reaction temperature 240 °C, MeOH/H₂O molar ratio of 0.56:1, mode II).

with elevating the S_V from 7.2 to 12.0 h⁻¹. Due to the reciprocal relationship between S_V and residence time, the increment of S_V can be regarded as the equivalent function of reducing the residence time for reactant. It tends to impair the methanol conversion for incomplete reaction. On the other side, the hydrogen yield was remarkably improved from 83.09 to 93.71% with the S_V ranging from 7.2 to 12.0 h⁻¹, owing to the enhancement of external diffusion for this gas–solid heterogeneous catalytic reaction by increasing the flow rate of reactant.

3.9. Effect of Reactant Molar Ratio. Figure 10 shows that the methanol conversion decreases with increasing the methanol/water molar ratio (MeOH/H₂O) from 0.56:1 to

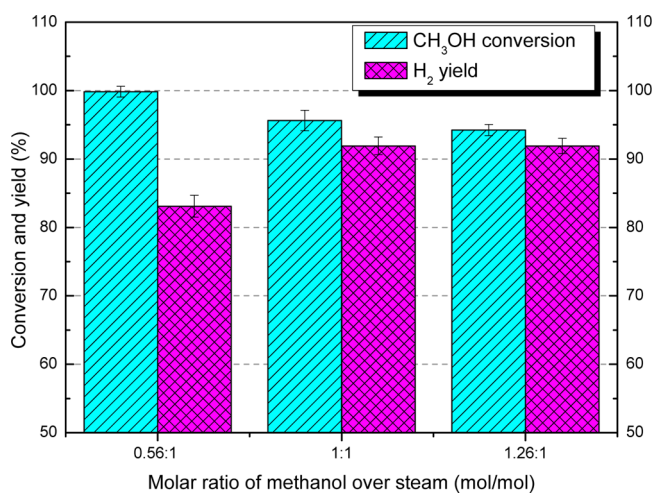


Figure 10. Effect of molar ratio of methanol over steam (reaction temperature 240 °C and S_V of 7.2 h⁻¹, mode II).

1:1 and 1.26:1, of which the change tendency is in good agreement with the literature report.³³ This is ascribed to less methanol taking part in the SRM reaction due to thermodynamic equilibrium by decreasing the mole fraction of water in feed. In addition, the use of excessive methanol would bring about more decomposition of methanol by forming more byproduct CO and carbon deposition.⁵⁶ Therefore, from the viewpoint of preferable methanol conversion, it is better to adopt a low MeOH/H₂O molar ratio. When the molar ratio departs from the stoichiometric coefficient ratio of 1:1, the reactive probability becomes slender for unit methanol molecules simultaneously contacting with steam and catalyst. As a result, the maximum value for hydrogen yield attains 91.92% at the MeOH/H₂O molar ratio of 1:1.

Actually, the reversible side reaction of water gas shift (WGS) would be enhanced at higher methanol conversion at lower methanol/water molar ratio or space velocity, from which the derived CO would either convert into coke or diminish the hydrogen purity in the product.³³ Therefore, the optimum operation condition is determined at streaming mode II for CCMs, together with a space velocity of 9.6 h⁻¹ and a methanol/water molar ratio of 1:1, when the methanol conversion and hydrogen yield could reach 95% and 92%, respectively.

It is worth noticing that the CCMs are also potentially favorable for maintaining their catalytic activity in air for a long time because the inert carbon matrix can prevent the embedded nanosized catalyst from being susceptible to surrounding species.⁵⁷ In summary, there is still a lot of room for the research and development of catalytic carbon membranes.

4. CONCLUSIONS

In this article, catalytic carbon membranes were fabricated by incorporating copper-based catalyst into a carbon membrane matrix. The nanosized catalyst particles are well dispersed in the matrix of carbon membranes. The addition of catalyst improves the thermal stability of the precursor and diminishes the porosity of the resultant carbon membranes. The reactor integrated by as-synthesized catalytic carbon membranes is more favorable for the intensification of the methanol steam reforming reaction in comparison to the reactors of inert carbon membranes and fixed bed. The reaction results in catalytic carbon membrane reactor follow the common rules of the traditional reactor, i.e., the methanol conversion being improved by decreasing the space velocity or the methanol/steam molar ratio. The carbon membrane matrix can boost the catalytic activity by providing good dispersion of catalyst and enhancing the transfer property of reactant. However, the additional pore diffusion resistance for reactant in catalytic carbon membranes should not be neglected. Further work is suggested to be carried out in terms of the effects of the structure and configuration of catalytic carbon membranes on the reaction of methanol steam reforming.

AUTHOR INFORMATION

Corresponding Authors

*E-mail: bzhangdut@163.com. Tel.: +(86)-419-5319450. Fax: +(86)-419-5311989.

*E-mail: wangth@dlut.edu.cn.

Notes

The authors declare no competing financial interest.

ACKNOWLEDGMENTS

This work was financially supported by the National Natural Science Foundation of China (20906063, 21176063, and 21376037), the National High-tech Research and Development Project of China (2012AA03A611), the Liaoning Natural Science Foundation of China (20102170), the Program for Liaoning Excellent Talents in University (LJQ2012010), and the State Key Laboratory of Fine Chemicals (KF1107).

REFERENCES

- (1) Dixon, R. K. Advancing Towards a Hydrogen Energy Economy: Status, Opportunities and Barriers. *Mitigation Adapt. Strategies Global Change* 2007, 12, 305.
- (2) Solomon, B. D.; Banerjee, A. A Global Survey of Hydrogen Energy Research, Development and Policy. *Energy Policy* 2006, 34, 781.
- (3) Palo, D. R.; Dagle, R. A.; Holladay, J. D. Methanol Steam Reforming For Hydrogen Production. *Chem. Rev.* 2007, 107, 3992.
- (4) Gallucci, F.; Paturzo, L.; Basile, A. Hydrogen Recovery from Methanol Steam Reforming In a Dense Membrane Reactor: Simulation Study. *Ind. Eng. Chem. Res.* 2004, 43, 2420.
- (5) Peppley, B. A.; Amphlett, J. C.; Kearns, L. M.; Mann, R. F. Methanol Steam Reforming On Cu/ZnO/Al₂O₃. Part 1. The Reaction Network. *Appl. Catal., A* 1999, 179, 21.
- (6) Peppley, B. A.; Amphlett, J. C.; Kearns, L. M.; Mann, R. F. Methanol Steam Reforming On Cu/ZnO/Al₂O₃ catalysts. Part 2. A Comprehensive Kinetic Model. *Appl. Catal., A* 1999, 179, 31.
- (7) Itoh, N.; Haraya, K. A Carbon Membrane Reactor. *Catal. Today* 2000, 56, 103.
- (8) Srnejer, G.; Sheintuch, M. Application of A Carbon Membrane Reactor for Dehydrogenation Reactions. *Chem. Eng. Sci.* 2004, 59, 2013.
- (9) Zhang, X.; Hu, H.; Zhu, Y.; Zhu, S. Methanol Steam Reforming to Hydrogen in a Carbon Membrane Reactor System. *Ind. Eng. Chem. Res.* 2006, 45, 7997.
- (10) Sá, S.; Sousa, J. M.; Mendes, A. Steam Reforming of Methanol over a CuO/ZnO/Al₂O₃ Catalyst Part II: A Carbon Membrane Reactor. *Chem. Eng. Sci.* 2011, 66, 5523.
- (11) Sá, S.; Silva, H.; Sousa, J. M.; Mendes, A. Hydrogen Production by Methanol Steam Reforming in a Membrane Reactor: Palladium vs Carbon Molecular Sieve Membranes. *J. Membr. Sci.* 2009, 339, 160.
- (12) Briceño, K.; Julianelli, A.; Montané, D.; Garcia-Valls, R.; Basile, A. Carbon Molecular Sieve Membranes Supported On Non-Modified Ceramic Tubes For Hydrogen Separation In Membrane Reactors. *Int. J. Hydrogen Energy* 2012, 37, 13536.
- (13) Lee, D.-W.; Park, S.-J.; Yu, C.-Y.; Ihm, S.-K.; Lee, K.-H. Study On Methanol Reforming-Inorganic Membrane Reactors Combined with Water-Gas Shift Reaction and Relationship Between Membrane Performance and Methanol Conversion. *J. Membr. Sci.* 2008, 316, 63.
- (14) Nam, J.-H.; Jang, Y.-Y.; Kwon, Y.-U.; Nam, J.-D. Direct Methanol Fuel Cell Pt-Carbon Catalysts by Using SBA-15 Nanoporous Templates. *Electrochim. Commun.* 2004, 6, 737.
- (15) Lin, M.-L.; Huang, C.-C.; Lo, M.-Y.; Mou, C.-Y. Well-ordered Mesoporous Carbon Thin Film with Perpendicular Channels: Application to Direct Methanol Fuel Cell. *J. Phys. Chem. C* 2008, 112, 867.
- (16) Jakobs, E.; Koros, W. J. Ceramic Membrane Characterization via the Bubble Point Technique. *J. Membr. Sci.* 1997, 124, 149.
- (17) Venkataraman, K.; Choate, W. T.; Torre, E. R.; Husung, R. D.; Batchu, H. R. Characterization Studies of Ceramic Membranes. A Novel Technique Using a Coulter Porometer. *J. Membr. Sci.* 1988, 39, 259.
- (18) Determination of Porosity of Porous Ceramics by Density Method. *China National Standard GB/T 1966–1996*; Sept 13, 1996.
- (19) Pérez-Hernández, R.; Gutiérrez-Martínez, A.; Espinosa-Pesqueira, M. E.; Estanislao, Ma. L.; Palacios, J. Effect of the Bimetallic Ni/Cu Loading on the ZrO₂ Support for H₂ Production in

- the Autothermal Steam Reforming of Methanol. *Catal. Today* **2014**, DOI: 10.1016/j.cattod.2014.08.009.
- (20) Mark, H. F. *Encyclopedia of Polymer Science and Technology*; Wiley-VCH Verlag GmbH: Weinheim, Germany, 2004; Vol. 7, p 341.
- (21) Zhang, B.; Shi, Y.; Wu, Y.; Wang, T.; Qiu, J. Preparation and Characterization of Supported Ordered Nanoporous Carbon Membranes for Gas Separation. *J. Appl. Polym. Sci.* **2014**, *131*, 2136.
- (22) Zhang, X.; Looney, M. G.; Solomon, D. H.; Whittaker, A. K. The Chemistry of Novolac Resins: 3. ^{13}C and ^{15}N n.m.r. Studies of Curing with Hexamethylenetetramine. *Polymer* **1997**, *38*, 5835.
- (23) Zhou, W.; Yoshino, M.; Kita, H.; Okamoto, K. Carbon Molecular Sieve Membranes Derived from Phenolic Resin with a Pendant Sulfonic Acid Group. *Ind. Eng. Chem. Res.* **2001**, *40*, 4801.
- (24) Elashmawi, I. S.; Hakeem, N. A.; Marei, L. K.; Hanna, F. F. Structure and Performance of ZnO/PVC Nanocomposites. *Physica B* **2010**, *405*, 4163.
- (25) Agarwal, V.; Patel, S.; Pant, K. K. H_2 Production by Steam Reforming of Methanol over $\text{Cu}/\text{ZnO}/\text{Al}_2\text{O}_3$ Catalysts: Transient Deactivation Kinetics Modeling. *Appl. Catal., A* **2005**, *279*, 155.
- (26) Bimbela, F.; Chen, D.; Ruiz, J.; García, L.; Arauzo, J. Ni/Al Coprecipitated Catalysts Modified with Magnesium and Copper for the Catalytic Steam Reforming of Model Compounds from Biomass Pyrolysis Liquids. *Appl. Catal., B* **2012**, *119–120*, 1.
- (27) Echegoyen, Y.; Suelves, I.; Lázaro, M. J.; Sanjuán, M. L.; Moliner, R. Thermo Catalytic Decomposition of Methane over Ni–Mg and Ni–Cu–Mg Catalysts: Effect of Catalyst Preparation Method. *Appl. Catal., A* **2007**, *333*, 229.
- (28) Pojanavaraphan, C.; Luengnaruemitchai, A.; Gulari, E. Catalytic Activity of Au–Cu– CeO_2 – ZrO_2 Catalysts in Steam Reforming of Methanol. *Appl. Catal., A* **2013**, *456*, 135.
- (29) Khzouz, M.; Wood, J.; Pollet, B.; Bujalski, W. Characterization and Activity Test of Commercial $\text{Ni}/\text{Al}_2\text{O}_3$, $\text{Cu}/\text{ZnO}/\text{Al}_2\text{O}_3$ and Prepared Ni–Cu– Al_2O_3 Catalysts for Hydrogen Production from Methane and Methanol Fuels. *Int. J. Hydrogen Energy* **2013**, *38*, 1664.
- (30) Trimm, D. L. Coke Formation and Minimization during Steam Reforming Reactions. *Catal. Today* **1997**, *37*, 233.
- (31) Benito, M.; Sanz, J. L.; Isabel, R.; Padilla, R.; Arjona, R.; Daza, L. Bio-Ethanol Steam Reforming: Insights on the Mechanism For Hydrogen Production. *J. Power Sources* **2005**, *151*, 11.
- (32) Twigg, M. V.; Spencer, M. S. Deactivation of Copper Metal Catalysts for Methanol Decomposition, Methanol Steam Reforming and Methanol Synthesis. *Top. Catal.* **2003**, *22*, 191.
- (33) Shimoda, N.; Muroyama, H.; Matsui, T.; Faungnawakij, K.; Kikuchi, R.; Eguchi, K. Dimethyl Ether Steam Reforming under Daily Start-Up and Shut-Down (DSS)-like Operation over CuFe_2O_4 Spinel and Alumina Composite Catalysts. *Appl. Catal., A* **2011**, *409–410*, 91.
- (34) Valdés-Solís, T.; Marbán, G.; Fuertes, A. B. Nanosized Catalysts for the Production of Hydrogen by Methanol Steam Reforming. *Catal. Today* **2006**, *116*, 354.
- (35) Rodriguez, N. M.; Kim, M. S.; Baker, R. T. K. Deactivation of Copper Nickel-Catalysts Due to Changes in Surface Composition. *J. Catal.* **1993**, *140*, 16.
- (36) Cesano, F.; Scarano, D.; Bertarione, S.; Bonino, F.; Damin, A.; Bordiga, S.; Prestipino, C.; Lamberti, C.; Zecchina, A. Synthesis of ZnO –Carbon Composites and Imprinted Carbon by the Pyrolysis of ZnCl_2 -Catalyzed Furfuryl Alcohol Polymers. *J. Photochem. Photobiol., A* **2008**, *196*, 143.
- (37) Li, L.; Song, L.; Wang, H.; Chen, C.; She, Y.; Zhan, Y.; Lin, X.; Zheng, Q. Water–Gas Shift Reaction Over CuO/CeO_2 Catalysts: Effect of CeO_2 Supports Previously Prepared by Precipitation with Different Precipitants. *Int. J. Hydrogen Energy* **2011**, *36*, 8839.
- (38) Li, L.; Zhan, Y.; Zheng, Q.; Zheng, Y.; Chen, C.; She, Y.; Lin, X.; Wei, K. Water–Gas Shift Reaction Over CuO/CeO_2 Catalysts: Effect of the Thermal Stability and Oxygen Vacancies of CeO_2 Supports Previously Prepared by Different Methods. *Catal. Lett.* **2009**, *130*, 532.
- (39) Li, L.; Zhan, Y.; Chen, C.; She, Y.; Lin, X.; Zheng, Q. Effect of CeO_2 Support Prepared with Different Methods on the Activity and Stability of CuO/CeO_2 Catalysts for the Water–Gas Shift Reaction. *Acta Phys. Chim. Sin.* **2009**, *25*, 1397.
- (40) Li, L.; Zhan, Y.; Zheng, Q.; Zheng, Y.; Lin, X.; Li, D.; Zhu, J. Water–Gas Shift Reaction over Aluminum Promoted Cu/CeO_2 Nanocatalysts Characterized by XRD, BET, TPR and Cyclic Voltammetry (CV). *Catal. Lett.* **2007**, *118*, 91.
- (41) Liu, Y.; Hayakawa, T.; Suzuki, K.; Hamakawa, S.; Tsunoda, T.; Ishii, T.; Kumagai, M. Highly Active Copper/Ceria Catalysts for Steam Reforming Of Methanol. *Appl. Catal., A* **2002**, *223*, 137.
- (42) Pojanavaraphan, C.; Nakaranuwattana, W.; Luengnaruemitchai, A.; Gulari, E. Effect of Support Composition and Metal Loading on $\text{Au}/\text{Ce}_{1-x}\text{Zr}_x\text{O}_2$ Catalysts for the Oxidative Steam Reforming of Methanol. *Chem. Eng. J.* **2014**, *240*, 99.
- (43) Faungnawakij, K.; Kikuchi, R.; Eguchi, K. Thermodynamic evaluation of methanol steam reforming for hydrogen production. *J. Power Sources* **2006**, *161*, 87.
- (44) Jeong, H.; Kim, K. I.; Kim, T. H.; Ko, C. H.; Park, H. C.; Song, I. K. Hydrogen Production by Steam Reforming of Methanol in a Micro-Channel Reactor Coated with $\text{Cu}/\text{ZnO}/\text{ZrO}_2/\text{Al}_2\text{O}_3$ Catalyst. *J. Power Sources* **2006**, *159*, 1296.
- (45) Ou, T.-C.; Chang, F.-W.; Roselin, L. S. Production of Hydrogen via Partial Oxidation of Methanol over Bimetallic Au–Cu/TiO₂ Catalysts. *J. Mol. Catal. A: Chem.* **2008**, *293*, 8.
- (46) Liu, W. Multi-Scale Catalyst Design. *Chem. Eng. Sci.* **2007**, *62*, 3502.
- (47) Twigg, M. V.; Spencer, M. S. Deactivation of Supported Copper Metal Catalysts for Hydrogenation Reactions. *Appl. Catal., A* **2001**, *212*, 161.
- (48) Shishido, T.; Yamamoto, Y.; Morioka, H.; Takaki, K.; Takehira, K. Active Cu/ZnO and $\text{Cu}/\text{ZnO}/\text{Al}_2\text{O}_3$ Catalysts Prepared by Homogeneous Precipitation Method in Steam Reforming of Methanol. *Appl. Catal., A* **2004**, *263*, 249.
- (49) Jones, S. D.; Hagelin-Weaver, H. E. Steam Reforming of Methanol Over CeO_2 - and ZrO_2 -Promoted Cu-ZnO Catalysts Supported on Nanoparticle Al_2O_3 . *Appl. Catal., B* **2009**, *90*, 195.
- (50) Purnama, H.; Girgsdies, F.; Ressler, T.; Schattka, J. H.; Caruso, R. A.; Schomäcker, R.; Schlögl, R. Activity and Selectivity of a Nanostructured CuO/ZrO_2 Catalyst in the Steam Reforming of Methanol. *Catal. Lett.* **2004**, *94*, 61.
- (51) Wang, L.-C.; Liu, Y.-M.; Chen, M.; Cao, Y.; He, H.-Y.; Wu, G.-S.; Dai, W.-L.; Fan, K.-N. Production of Hydrogen by Steam Reforming of Methanol over Cu/ZnO Catalysts Prepared via a Practical Soft Reactive Grinding Route Based on Dry Oxalate-Precursor Synthesis. *J. Catal.* **2007**, *246*, 193.
- (52) Iulianelli, A.; Ribeirinha, P.; Mendes, A.; Basile, A. Methanol Steam Reforming for Hydrogen Generation via Conventional and Membrane Reactors: A Review. *Renewable Sustainable Energy Rev.* **2014**, *29*, 355.
- (53) Hatori, H.; Kobayashi, T.; Hishiki, S.; Yamada, Y.; Matsuno, S.; Nishio, T. Nano-space Structure of Carbon from Polyimide Containing Nickel Nitrate and Their Function on Catalytic Reaction. *Synth. Met.* **2001**, *125*, 183.
- (54) Shi, Y.; Du, X.; Yang, L.; Sun, Y.; Yang, Y. Experiments on Hydrogen Production From Methanol Steam Reforming in Fluidized Bed Reactor. *Int. J. Hydrogen Energy* **2013**, *38*, 13974.
- (55) Wang, G.; Wang, F.; Li, L.; Zhang, G. Experimental Investigation of Axially Non-Uniform Catalysis For Methanol Steam Reforming. *J. Power Sources* **2014**, *250*, 306.
- (56) Wu, Y. J.; Diaz Alvarado, F.; Santos, J. C.; Gracia, F.; Cunha, A. F.; Rodrigues, A. E. Sorption-Enhanced Steam Reforming of Ethanol: Thermodynamic Comparison of CO_2 Sorbents. *Chem. Eng. Technol.* **2012**, *35*, 847.
- (57) Ruoff, R. S.; Lorents, D. C.; Chan, B.; Malhotra, R.; Subramoney, S. Single Crystal Metals Encapsulated In Carbon Nanoparticles. *Science* **1993**, *259*, 346.